WATER RESEARCH 45 (2011) 4571–4582

Available at www.sciencedirect.com

ScienceDirect

journal homepage: www.elsevier.com/locate/watres

Of microparticles and bacteria identification – (resonance) Raman micro-spectroscopy as a tool for biofilm analysis

Ann-Kathrin Kniggendorf[*], *Merve Meinhardt-Wollweber*[1]

Gottfried Wilhelm Leibniz University of Hannover, Institute of Biophysics, Herrenhäuser Str. 2, 30149 Hannover, Germany

ARTICLE INFO

Article history:
Received 22 March 2011
Received in revised form
28 May 2011
Accepted 4 June 2011
Available online 14 June 2011

Keywords:
Confocal Raman microscopy
Imaging
Native samples
Biofilms
Mineral particles
Uncultured microorganisms

ABSTRACT

Confocal resonance Raman microscopy is a powerful tool for the non-invasive analysis of complex biological aggregates without preparation and prior knowledge of the samples. We present the capabilities of confocal resonance Raman microscopy with a spatial resolution of 350 $nm^2 \times 2.0$ μm and excitation times of 1 s and less per recorded spectrum. Granules sampled from two sequencing batch reactors (SBR) for anaerobic ammonium oxidization (anammox) were regularly mapped in vivo for three months after SBR startup. Uncultured microorganisms and mineral particles were tracked throughout operation and identified in situ by their (resonance) Raman spectra. Co-existing microcolonies of *Nitrosomonae* formed the outer layer of anammox granules. Polymorph TiO_2 microparticles were found embedded in the outer layer of granules overgrown with purple bacteria, indicating bacterial response to the variant toxicity of the mineral phase.

1. Introduction

The analysis of complex microbial aggregates and multi-species biofilms is still a challenge even for advanced imaging and identification techniques. These aggregates are formed of dense, highly hydrated, highly structured clusters of bacterial cells bound together by extracellular polymeric substances (EPS). Such clusters – so called microcolonies – differ in the bacterial species or phenotype of the species clustered together. In addition, a majority of the bacteria associated in biofilms cannot be grown in a pure culture, deferring most – if not all – standard-techniques for bacterial identification. Even those species for which pure cultivation is possible often show distinctly different phenotypic traits in a biofilm than seen in their planctonic culture (Steward and Franklin, 2008).

Understanding these complex communities requires advanced non-destructive imaging techniques providing information on spatial structure and distribution of – as well as tracking and identification capabilities for – the microorganisms associated in them, preferably without requiring invasive preparations or prior knowledge of the sample. Raman micro-spectroscopy – successfully used for the in vivo mapping of biofilms as well as identification and taxonomy of bacteria – is among the most promising techniques proposed for these tasks (Sandt et al., 2007; Harz et al., 2008). However, it

[*] *Corresponding author*. Present address: Gottfried Wilhelm Leibniz University of Hannover, Institute of Quantumoptics, Welfengarten 1, 30167 Hannover, Germany. Tel.: +49 511 762 5125; fax: +49 511 762 19432.
E-mail addresses: kniggendorf@iqo.uni-hannover.de (A.-K. Kniggendorf), merve.wollweber@hot.uni-hannover.de (M. Meinhardt-Wollweber).
[1] Present address: Gottfried Wilhelm Leibniz University of Hannover, HOT - Hannoversches Zentrum für Optische Technologien, Nienburger Str. 17, 30167 Hannover, Germany.
0043-1354/$ – see front matter © 2011 Elsevier Ltd. All rights reserved.
doi:10.1016/j.watres.2011.06.007

suffers from long measurement times and a high sensitivity to environmental (or culture) conditions, making it difficult to apply on extended segments of biofilm and bacteria in various habitats. To overcome these limitations, Raman micro-spectroscopy has been combined with several other methods, such as confocal laser scanning microscopy (CLSM) (Wagner et al., 2009), environmental scanning electron microscopy (ESEM) (Schwartz et al., 2009), and even fluorescent in situ hybridization (FISH) (Huang et al., 2007).

However, by employing molecular resonances of inherent and ubiquitous but specific chromophores in confocal Raman microscopy, it is possible to achieve an in-depth analysis of the targeted microbial communities without additional, more invasive techniques or prior knowledge of the sample being required. The omnipresent autofluorescent background seen in biofilms at visible excitation wavelengths returns structural and morphologic information even in the rare case of absent chromophores thus preventing false negatives. In the presence of chromophores, information about structure, water content, bacteria (tracking, identification, and distribution), and non-biological components such as mineral microparticles is accessible on the scale of single cells (approx. 1 μm^3).

As an example, we analyzed the outer layer of bacterial aggregates sampled over three months from two identical sequencing batch reactors (SBR) for anaerobic ammonium oxidization (anammox) – one showing nominal anammox operation and one severely infected with purple bacteria – with confocal (resonance) Raman micro-spectroscopy at 532 nm excitation.

2. Materials and methods

2.1. Sequencing batch reactors (SBR)

Sample granules were provided by two sequencing batch reactors for the anammox process, each with a 12.8 l volume of which 10 l was used in operation. The SBRs were started with UASB pellets from an industrial IC reactor in Germany, treating the wastewater of an ethanol distillery, and active sludge from the municipal wastewater treatment plant in Hanover, Germany, in a ratio of 1:1. SBR-1 was additionally inoculated with seeding sludge from an operational anammox-IC in Rotterdam (Van der Star et al., 2008). Construction and operation of the SBRs were otherwise identical. SBR-1 was previously described and characterized by Wesoly (2009). It showed steady anammox activity after a startup phase of approx. two weeks. The main anammox organism present was *candidatus Brocadia anammoxidans*, tested with the FISH probe Ban162 (Wesoly, 2009).

SBR-0 showed an increasing population of not otherwise specified purple bacteria after three weeks of operation. SBR-0's operation was discontinued after three months when no anammox occurred, while SBR-1 was kept in operation and monitored for another six months, showing steady anammox activity.

Both SBRs were monitored in 48 h intervals with resonance Raman measurements as described in 2.3.1. A 3D image as described in 2.3.2 was recorded every 96 h. Identical measurements were performed on granules of the seeding sludge prior to inoculation.

Samples for subsequent resonance Raman measurements were taken from the SBRs always at the same phase of the operation cycle (during stirring). 50 ml of reactor water including microbial granules were sampled with a wide syringe at half-height from each SBR immediately prior to measurements.

A single granule of average size (diameter: ~1 mm) was taken from the sampled volume and placed free-floating in ample bulk liquid on an uncoated 1.2 mm indentation slide. The cover slip was sealed with acrylic lacquer to the slide to avoid dehydration of the sample. Measurements were started 2 min after sealing (to allow for drying of the sealing lacquer).

2.2. Bacterial cultures and reference chemicals

Four strains of *Nitrosomonae* expressing cytochrome-c – *Nitrosomonas communis* Nm-02, two strains of *Nitrosomonas europaea* (Nm-50, Nm-53), and *Nitrosomonas eutropha* Nm-57 provided as liquid cultures by Dr. Pommerening-Röser of the Biozentrum Klein Flottbek, Hamburg, Germany – were cultured using media and conditions as described by Koops et al. (1991).

Rhodobacter sphaeroides DSM 158^T producing spheroidene and cytochrome-cbb_3 and its carotenoids-free mutant DSM 2340^T expressing only cytochrome-cbb_3 were obtained as freeze-dried cultures from the German Collection of Microorganisms and Cell Cultures (Deutsche Sammlung von Mikroorganismen und Zellkulturen [DSMZ]), Braunschweig, Germany and cultured as described in Kniggendorf et al. (2011). Carotenoid production – or the lack thereof – was tested spectrometrically (Kontron Uvikon 932). Samples for subsequent Raman measurements were prepared and measured as previously described in Kniggendorf et al. (2011a).

99% pure cytochrome-c from bovine heart was obtained from Sigma–Aldrich Chemie GmbH, Munich, Germany.

2.3. Confocal resonance Raman measurements

Resonance Raman measurements were performed at room temperature with a confocal Raman microscope (CRM200, by WITec GmbH, Ulm, Germany), equipped with a water-immersion objective (Nikon CFI Fluor) with a magnification of 60, and a Numerical Aperture of 1.0. A stabilized, frequency-doubled continuous-wave Nd:YAG laser at 532 nm was used for excitation. Photons from Rayleigh scattering were blocked with an edge filter, covering the range from −120 to 120 rel. cm^{-1}. The system has an ellipsoid measurement volume of approx. 1 μm^3 defined by the lens properties (assumed refractive index within the sample: 1.33 (water)). The spatial resolution in the horizontal plane was 350 nm and 2.0 μm perpendicular to it, tested experimentally on glass/chromophore-sample transitions. Slit width was 50 μm, realized by a multimode fiber connecting the Raman microscope with the spectrometer (Acton 308-SP). The spectrometer was equipped with two computer-controlled detection units – a backthinned CCD camera (Andor DU401-BV), electrically

cooled to −70 °C for spectrally resolved detection, and a single-photon sensitive Avalanche photodiode (APD; SPCM-AQR) – selectable via an adjustable mirror. The used grating had 600 lines per millimeter. Laser intensity was adjusted to 9 mW, giving 2.3 MW/cm^2 on the sample within the measurement volume.

2.3.1. *Spectral imaging*

Measurement time per spectrum (or recorded pixel) was set to 1.0 s, sufficient for high-contrast resonance Raman spectra of cytochrome-c. Recorded images consisted of 140 × 80 spectra screening an area of 70 μm horizontally and 80 μm vertically (into the granule). The spectral resolution of the setup was 4 cm^{-1} with a spectral accuracy of 2 cm^{-1}. Recorded spectrum range was −125 to 3694 rel. cm^{-1}.

2.3.2. *3D imaging*

Measurement time per recorded pixel was set to 0.1 s. The setup recorded a section of approx. 4 cm^{-1} around the denoted center frequency with a spectral accuracy of 2 cm^{-1}, allowing for specifically targeting resonantly enhanced Raman lines.

Recorded image stacks consisted of 80 images distanced 1 μm along the z-axis (vertically into the granule). Each image consisted of 300 × 300 spectra, covering an area of 100 × 100 μm^2 in the xy-plane.

2.4. *Spectral image analysis*

Spectral images were recorded with ScanCTRL plus and digitally analyzed with WITec Project 1.94, both by WITec GmbH, Ulm, Germany. Image dimensions mimic the scanned micrometer range, not the number of recorded pixels. Since each recorded pixel contains full spectral information – autofluorescent background as well as possible Raman spectra – two different sets of filters were used to extract information and generate informative images from the recorded data.

Broadband image filters are independent of whether or not Raman active chromophores are present. They display a sectioned superposition of the always present background and possible Raman spectra, allowing to mark areas of pure autofluorescence and/or high water content. For this, the recorded spectrum range was divided into three disjoint regions with region I going from 200 to 1300 cm^{-1} (colored red), region II from 1300 to 2400 cm^{-1} (yellow), and region III from 2400 to 3500 cm^{-1} (blue). Fig. 1(a) gives the spectral sectioning for broadband filters superimposed on an exemplary set of (resonant) Raman spectra.

Maximum and minimum intensity were defined per filtered image as the brightest and darkest pixel, with the darkest pixel being set to "black" (maximum contrast), resulting in a superimposition of the three filtered images ("broadband image") giving white in case of plain fluorescence (same intensity in all three regions), blue in case of high water content due to the wide Raman band consisting of unresolved OH-stretching modes above 3000 cm^{-1}, and monochrome, unstructured red in case of glasses with homogenous density (for example microscope slides or cover slips).

Microbial content shows as structured red and purple in a broadband image, due to the main intensity of bacterial spectra being primarily in broadband section I (red) and less in II (yellow). The water content of low density biofilm matter gives a low intensity in III (blue), resulting in a dark blue coloring (or purple in case of bacteria being present).

Mineral microparticles, having Raman spectra with comparatively low intensity and no fluorescent background do not show in broadband images, except as dark areas with little to no intensity.

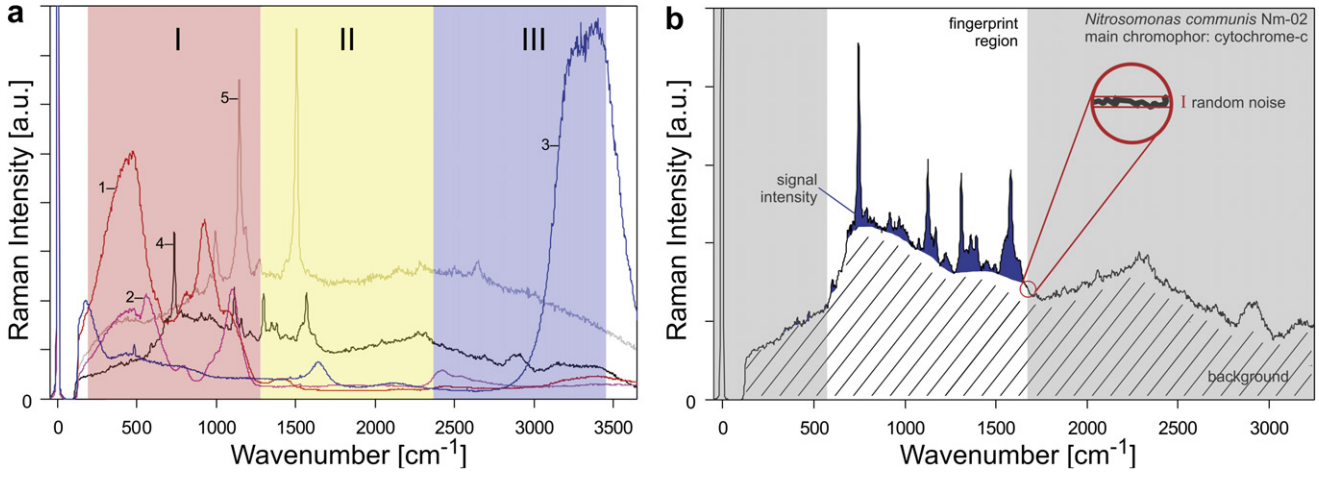

Fig. 1 – Filter concepts for spectral imaging. Broadband image filters (a) are independent of a chromophore being detected. The full spectrum as recorded is divided into three equal regions: 200–1300 cm^{-1} (I – red), 1300–2400 cm^{-1} (II – yellow), and 2400–3500 cm^{-1} (III – blue). Included (resonant) Raman spectra are glass of a microscope slide (1) and a cover slip (2), water (3), *Nitrosomonas communis* Nm-02 (chromophore: cytochrome-c) (4), and *Rhodobacter sphaeroides* DSM 158^T (chromophore: spheroidene) (5). Fingerprint image filters (b) return the distribution and intensity of a specific (resonance) Raman spectrum within the recorded spectral image. For their construction the shaded parts of the spectrum are cut and the autofluorescent background (hatched) is subtracted. (For interpretation of the references to colour in this figure legend, the reader is referred to the web version of this article).

Fingerprint image filters give the distribution of a specific Raman spectrum within the recorded spectral image. Fingerprint image filters were constructed from the fingerprint region of Raman spectra found recurrently in the spectral images (including various types of unidentified bacteria and microparticles).

Raman spectra of mineral microparticles were identified via RRUFF™ (Downs, 2006) and used in their entirety due to their negligible background and low number of Raman lines.

Fingerprint image filters for more complex Raman spectra with noticeable autofluorescent background – as for example seen in spectra of bacteria expressing cytochrome-c as main chromophore – were prepared as follows: The spectra were cut to the fingerprint region (600–1800 cm^{-1} throughout this work), followed by a full background reduction (9th order polynomial fit) over the same region (Fig. 1(b)). Intensity of a specific Raman line has to exceed the random noise by at least a factor of two to be considered as signal.

Maximum intensity was set for the pixel holding the strongest Raman spectrum with respect to the four most intense Raman lines within the fingerprint region. Minimum intensity ("black") was set for the four strongest Raman lines of the respective filter not exceeding background intensity.

Fingerprint images were constructed by superimposing the fingerprint filtered images of interest. Colors were chosen with respect to visibility. The number of fingerprint filters usable on a recorded spectral image is virtually unlimited, but the number of fingerprint filtered images that can be included in a single superimposition ("fingerprint image") is limited by the number of available colors and the limitations of additive color blending. However, an unlimited number of different fingerprint images can be created for a recorded spectral image.

2.5. *Raman spectra comparison (OPUS IDENT) and hierarchical cluster analysis (HCA)*

Preparation and analysis of the Raman spectra was done with commercial spectra analysis software (OPUS version 5.5 including IDENT by Bruker). Spectrum properties were determined and bacterial references compiled as previously described in Kniggendorf et al. (2011a). The critical random noise property is additionally illustrated in the inset of Fig. 1(b).

As a standard preparation of spectral HCA, the allowed spectral-to-noise ratio (S/N) was limited. Only Raman spectra with an S/N between 15 and 25 were used for further analysis to prevent differences in spectrum quality from exceeding variations caused by the actual bacteria.

All spectra were cut to the fingerprint region of 600–1800 cm^{-1} (the unshaded area in Fig. 1(b)), holding the most prominent peaks of the resonantly enhanced Raman spectrum of cytochrome-c, and vector-normalized to the same region. Spectral distances were calculated with the Euclidian Distance measurement. The initial vector-normalization limits the possible spectral distance to 2 (diameter of the unit ball) with a distance of 2 indicating an inverse spectrum and 0 indicating absolute identity (a spectrum being compared to itself).

Hierarchical cluster analyses were performed as described in Kniggendorf et al. (2011a) for single spectra with the Weighted-Average-Linkage algorithm.

3. Results

Fig. 2 shows a typical set of three spectral images for SBR-0 (purple bacteria) recorded after one month of operation: full spectral intensity as recorded (a), broadband image (b), and fingerprint image (c). The corresponding Raman spectra with the color-coding for Fig. 2(c) are given in Fig. 3. A similar set of spectral images for SBR-1 (anammox) recorded after one month of operation is given in Fig. 4 with the color-coded Raman spectra for Fig. 4(c) being given in Fig. 5.

3.1. *Chromophore identification*

The main chromophores found in Raman spectra from the outer layer of granules sampled from SBR-0 were identified as carotenoids with a spheroidene backbone (most intense Raman line at 1519 cm^{-1}; bacterial spectrum given in Fig. 3, spectrum (2), magenta) or a neurosporene backbone (most intense Raman line at 1526 cm^{-1}; bacterial spectrum given in Fig. 3, spectrum (1), blue).

Whereas the main chromophore found in the Raman spectra recorded in the outer layer of granules sampled from SBR-1 was heme-c as part of cytochrome-c. Cytochrome-c, resonantly enhanced in the Q-band, allows for the tracking (described below in 3.3) and identification (3.4) of bacteria in the biofilm. See spectra (1) to (3) in Fig. 5 for examples.

These substances were initially identified by their Raman spectra. Spheroidene was additionally confirmed by measuring a culture of *R. sphaeroides* DSM 158^T (data not shown), producing spheroidene as confirmed by absorption spectroscopy (data not shown). Cytochrome-c was additionally confirmed by comparison to a measurement of the pure substance (99% pure cytochrome-c from bovine heart) (data not shown).

Unexpectedly, the Raman spectra of two phases of mineral TiO_2 were found recurrently: Rutile (Fig. 3, spectrum (3), red) forming acicular or prismatic crystals, and anatase (Fig. 3, spectrum (4), yellow) in its typical form of dipyramidal or planar crystals.

Raman spectra occurring only isolated and in low numbers in the three months of measurements were considered natural impurities and ignored in further analysis.

3.2. *Spatially resolved information: structure and content*

3.2.1. *Structure of the outer layer*

As can be seen already in the full intensity images (Fig. 2(a) and Fig. 4(a)), the outer layers of the two SBRs are distinctly different from each other, with the outer layer of the granules from SBR-0 (Fig. 2(a)) being less regularly structured and of smaller overall width than that found in anammox granules sampled from SBR-1 (Fig. 4(a)). The microcolonies in granules sampled from SBR-0 form a haphazard monolayer with wide, irregular gaps, while the microcolonies seen in SBR-1 granules

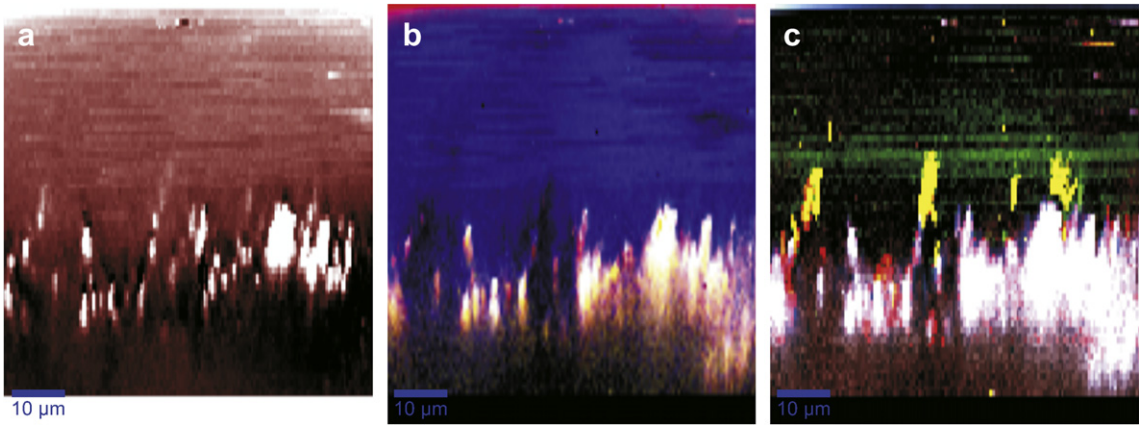

Fig. 2 – Spectral Imaging based on (resonance) Raman spectra (SBR-0 infested with purple bacteria). Set of three spectral images of the outer layer of a granule sampled after one month of operation from SBR-0 (infested with purple bacteria): full spectral intensity as recorded (a), broadband image (b), and fingerprint image (c). The broadband image (b) shows wide, water-rich gaps in a single layer of elongated microcolonies with intense autofluorescence (white) at their core covered by a thin layer of Raman-active bacteria (purple). The wide gaps contain substances with very low spectral intensity (black) and are filled and covered by a thick layer of low density biomass (dark blue). Yellow is indicative of the main spectral intensity being between 1300 and 2400 cm^{-1}, typically caused by Raman spectra with additional autofluorescence in the spectrum. The fingerprint image (c) reveals anatase microparticles (yellow) in the gaps and microcolonies of purple bacteria holding spheroidene (magenta), growing at and around rutile microparticles (red) and a thin cover of neurosporene producing bacteria (blue) especially on surfaces exposed to the bulk water. The green "streaks" in the bulk water are caused by free-floating cells without active chromophores, dragged along by the laser focus. The (resonant) Raman spectra in the respective color-coding are given in Fig. 3. (For interpretation of the references to colour in this figure legend, the reader is referred to the web version of this article).

are ordered in a dense multilayer with well-defined borders and few distinct canals into the depth of the granule. The width of these canals in SBR-1 seldom exceeded 3 µm. 3D images, recorded as described in 2.3.2, revealed the distance between adjacent bacterial microcolonies to seldom exceed 0.5 µm in granules sampled from SBR-1 (see Fig. 6), whereas microcolonies in granules from SBR-0 were distanced 1 µm and more from one another (Fig. 2).

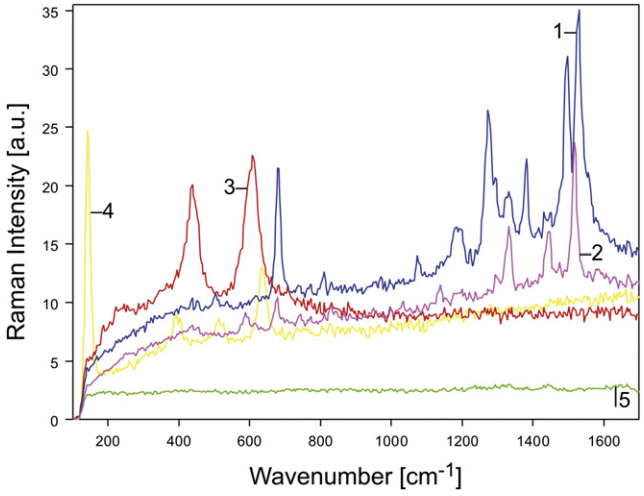

Fig. 3 – (Resonant) Raman spectra color-coded as in Fig. 2(c): (1) Purple bacteria producing neurosporene (Fig. 2(c) blue), (2) purple bacteria producing spheroidene (Fig. 2(c) magenta), (3) TiO_2 in rutile phase (Fig. 2(c) red), (4) TiO_2 in anatase phase (Fig. 2(c) yellow), and (5) a bacterial cell containing no chromophores (Fig. 2(c) green). Spectra are presented as recorded. (For interpretation of the references to colour in this figure legend, the reader is referred to the web version of this article).

3.2.2. *Discriminating autofluorescence, water, and biomass*

The broadband image of the granule sampled from SBR-0 (Fig. 2(b)) revealed strong autofluorescence (white) at the core of the microcolonies and large gaps of approx. 8–10 µm width in the outer layer, filled with water (blue) and water-saturated, low density biomass (dark blue).

Fig. 4(b) shows the broadband image recorded from the outer layer of the granule sampled from SBR-1. Only a comparatively small area on the surface shows slight autofluorescence (white). The low intensity of the fluorescent area can be seen by comparison with the image of full intensity as recorded (Fig. 4(a)). The canals of approx. 3 µm width are filled with water (blue). The outer layer traversed by these canals is formed of microbial colonies (red; purple colonies have a noticeable water content, confirmed via the respective Raman spectra).

3.2.3. *Analyzing microbial communities – who's where?*

The elongated microcolonies seen already in the full intensity images of both SBRs (see 3.2.1) are distinctly different from each other in their resonant Raman signatures.

The main chromophores found in the bacteria forming the microcolonies in the outer layer of SBR-0 granules were carotenoids of the spheroidene and neurosporene group. As seen in Fig. 2(c), individual bacterial colonies typically had a width of approx. 2–3 µm in the xy-plane and a length of

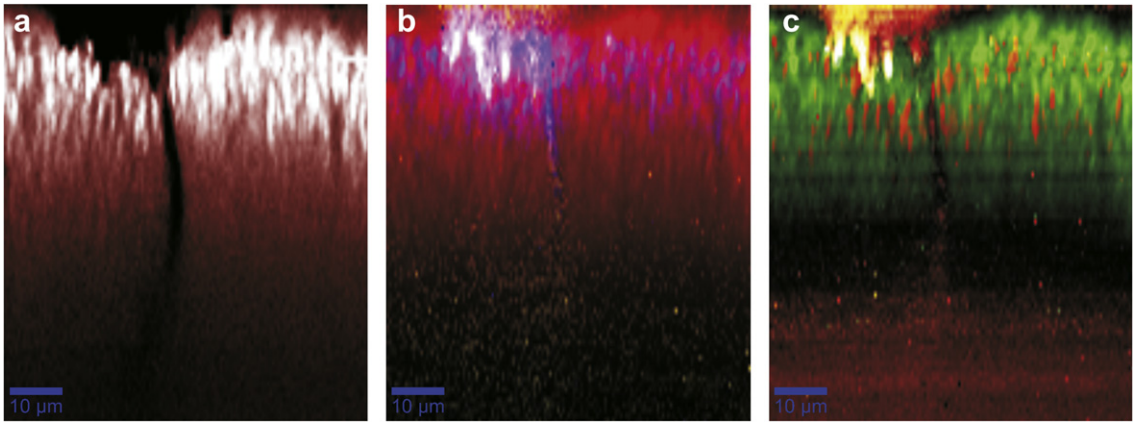

Fig. 4 – Spectral Imaging based on (resonance) Raman spectra (SBR-1 with nominal anammox activity). Set of three spectral images of the outer layer of a granule sampled after one month of operation from SBR-1 (anammox): full spectral intensity as recorded (a), broadband image (b), and fingerprint image (c). The outer layer of the granule sampled from SBR-1 shows a dense multilayer of microcolonies crossed centrally by a vertical canal (a second canal is touched near the right border of the image) already visible in the full spectral information (a). The broadband filtering (b) revealed water (blue) within the canal and the top third of the multilayer as well as weak autofluorescence (white; yellow in the presence of additional Raman lines) to the left of the bulk water opening of the canal. Fingerprint filtering (c) showed two types of *Nitrosomonas* microcolonies: *N. communis* (green) and a second species, probably *N. europaea*, (red). The corresponding resonance Raman spectra in the respective color-coding are given in Fig. 5. (For interpretation of the references to colour in this figure legend, the reader is referred to the web version of this article).

approx. 6–15 µm in the z-direction of the image. Only one layer of colonies was typically observed, spanning the whole width of the outer layer. The strong autofluorescent background made it impossible to detect Raman signals in the core of these microcolonies. However, all microcolonies showed purple bacteria producing primarily spheroidene (magenta, spectrum (2) in Fig. 3) on their surfaces, and often an additional thin layer of bacteria producing neurosporene (blue, spectrum (1) in Fig. 3) on surfaces exposed directly to bulk water. The latter were also seen on the walls of the wide, water-filled gaps.

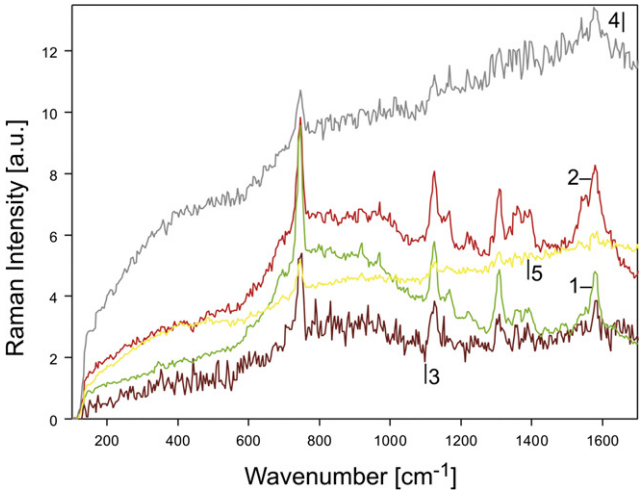

Fig. 5 – (Resonant) Raman spectra color-coded as in Fig. 4(c): (1) seed fingerprint type-I identified as *Nitrosomonas communis* (Fig. 4(c) green), (2) seed fingerprint type-II, probably *N. europaea*, (Fig. 4(c) red), (3) cytochrome-c spectrum 80 µm below the surface (Fig. 4(c) brown), (4) weak autofluorescence (Fig. 4(c) white), and (5) weakest autofluorescence (Fig. 4(c) yellow). (For interpretation of the references to colour in this figure legend, the reader is referred to the web version of this article).

In contrast, the nitrification zone of the granules sampled from SBR-1 was formed by multiple, interwoven layers of two types of bacterial colonies of similar appearance (width: 2–3 µm, length: up to 5 µm in the image), distinct only in their resonant Raman fingerprint: Type-I (green, spectrum (1) in Fig. 5) and the much rarer Type-II (red, spectrum (2) in Fig. 5). Bacteria of Type-I formed the main bulk of the microcolonies (green), while Type-II (red) was much rarer and always surrounded by densely packed Type-I colonies without direct contact to the granule surface or water-filled canals (Fig. 4(c)). The main chromophore of both types was cytochrome-c, allowing for species-sensitive tracking and identification of the bacteria (see 3.3 and 3.4 below).

Additional bacterial Raman spectra of cytochrome-c were detected underneath the nitrification zone (dark red, spectrum (3) in Fig. 5) and could be traced as deep as 80 µm into the granule. However, the quality of these spectra was not sufficient for a reliable comparison to the bacteria found within the nitrification layer.

Variant thickness of the nitrification zone was typically caused by increased distance between the microcolonies of the outer layer, i.e. the space between the microcolonies widened and filled with water and low density biomass (blue and dark blue in Fig. 7(b)). This can be seen by comparing Figs. 4, 6, and 7. Also note that Type-II colonies (red) are virtually absent from the thick, water-rich nitrification zone seen in Fig. 7(c).

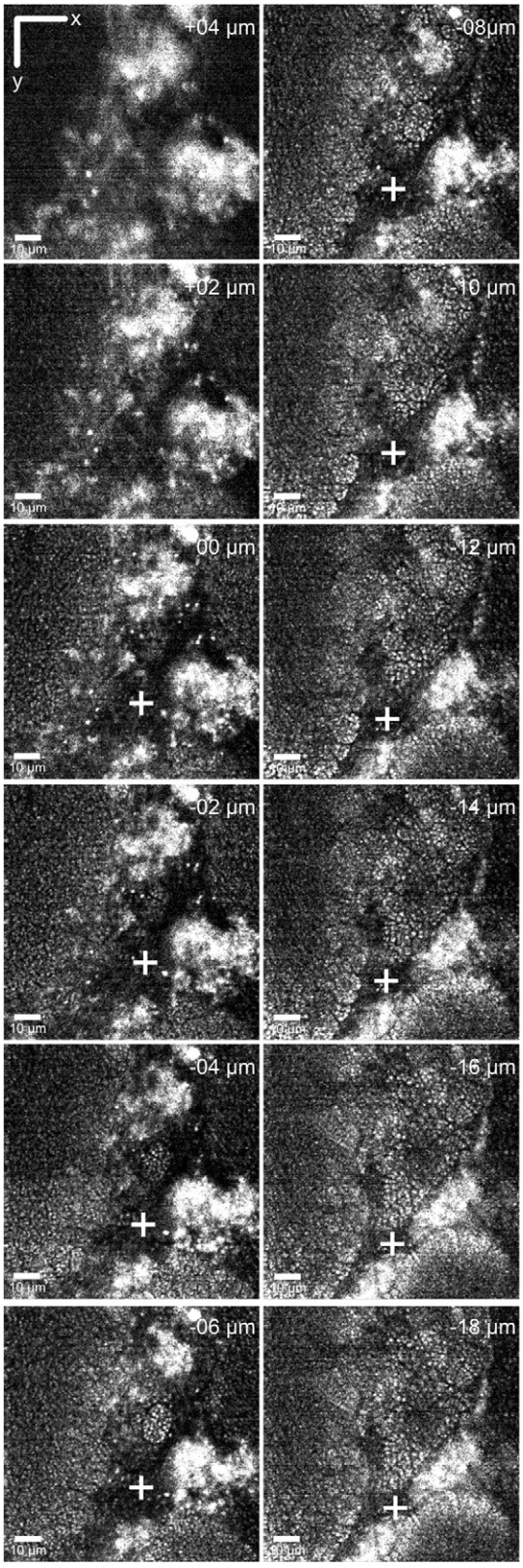

Fig. 6 – Excerpt of an image stack covering 100 × 100 × 20 µm³ of the outer layer of an anammox granule showing a canal (+). Every second image is shown; images below −20 µm were ignored; altitude was set to 0 µm for the first focused layer of cells; center frequency: 749 cm⁻¹ (pyrrole breathing, the strongest line of cytochrome-c at 532 nm excitation); excitation time per pixel: 0.1 s.

3.2.4. *Microparticles*

A noticeable amount of microparticles – TiO_2 in rutile and anatase phase – of a size up to 10 µm (average diameter was approx. 3 µm) were unexpectedly found in the outer layers of granules sampled from SBR-0 infested with purple bacteria. It is noteworthy, that these mineral particles have characteristic Raman lines at low wavenumbers, making them easily detectable even against increased autofluorescence as seen in the cores of purple bacteria colonies. The Raman spectrum of rutile (spectrum (3) in Fig. 3, red) consists of two lines at 447 and 613 cm^{-1}, while the spectrum of anatase (spectrum (4) in Fig. 3, yellow) has four lines with the strongest line as low as 144 cm^{-1} (the others being at 394, 514, and 638 cm^{-1} respectively).

In SBR-0 (Fig. 2(c)), pyramidal and tabular anatase crystals (yellow) were found only on the surface of the outer layer, often partially embedded in low density matter (visible as less intense water content (dark blue) in Fig. 2(b)) and without direct contact to bacterial microcolonies. In contrast, short sections of rutile prisms and needles (red) were typically found embedded in the outer layer and often thickly packed with microcolonies of spheroidene producing purple bacteria.

The outer layer of granules sampled from SBR-1 held only a few rutile microparticles and virtually no anatase was detected throughout the monitoring, discounting free particles in the bulk water (data not shown).

3.3. *Bacterial tracking – who stays?*

The two distinct Raman fingerprints of bacteria – Type-I and Type-II – found in the nitrification zone of granules sampled from SBR-1, were already found in abundance in the anammox seed granules obtained from Rotterdam and tracked successfully throughout operation of SBR-1. As seen in 3.2.3, these bacteria formed the majority of microcolonies in the outer layer of the granules sampled from SBR-1 (Fig. 4(c) and 7(c)) and of the seed granules obtained from Rotterdam (data not shown). Bacterial fingerprint Type-I (green) corresponded to spectrum (1) and Type-II (red) to spectrum (2) in Fig. 5. The respective Raman spectra recorded from the seed granules are given in Fig. 8.

Fig. 9 shows the hierarchical cluster analysis of a typical set of bacterial Raman single spectra extracted from various measurements made at different times during the operation of SBR-1 together with two sample spectra obtained from the seed granules (seed I and II). Resonant Raman spectra were identified with the fingerprint image filters (see 2.4) for Types-I and –II and exported from the respective spectral images. Spectra with a suitable signal-to-noise ratio were subsequently subjected to HCA as described in 2.5. Spectra were labeled with the date of the measurement (mmdd) and the type as identified by the fingerprint image filters.

As can be seen in Fig. 9, the two types of bacterial Raman spectra, classified as Type-I and –II by the fingerprint filters, were separated properly with a spectral distance larger than 0.7 between the branches I and II. Spectral distances between the components of a branch ranged from 0.25 to 0.46, with branch I forming a homogenous structure (spectrum 0903 has a stronger similarity to the seed 0801 and spectrum 0820 than

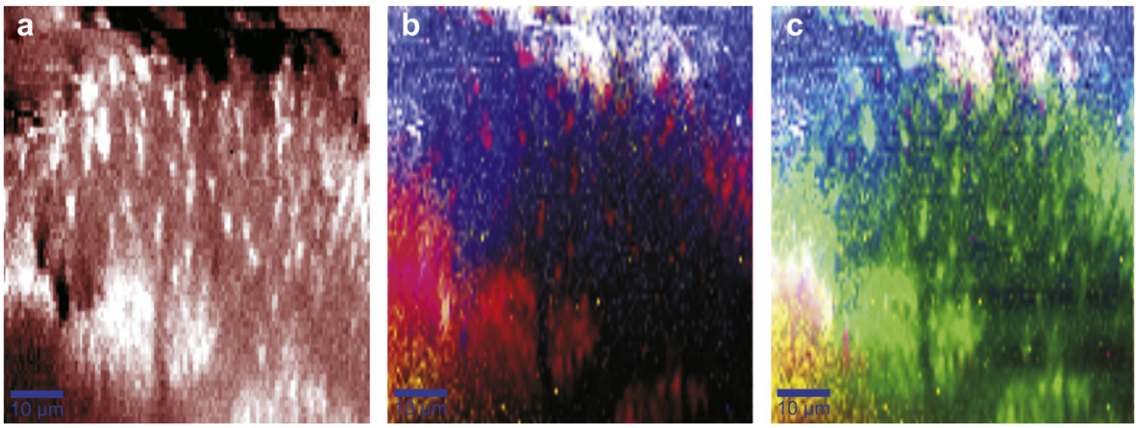

Fig. 7 – Spectral images based on resonance Raman spectra of an anammox granule swollen with water: full spectral intensity as recorded (a), broadband filtered image (b) categorizing bacteria (red, magenta), water (blue), low density biomass (dark blue), and autofluorescence (white), and fingerprint image (c) showing primarily green microcolonies of the tracked bacteria type-I (*Nitrosomonas communis*), very few bacteria of type-II (red), and weak autofluorescence (white) at the surface and right beneath the outer layer on the left. Filtered spectra are the same as in Fig. 4(c) and are given in Fig. 5. (For interpretation of the references to colour in this figure legend, the reader is referred to the web version of this article).

to 1022, as indicated by the corrective numbers underneath the respective clusters) and branch II being divided into a starting cluster (0801, 0813, 0830) including the seed and spectra recorded within the first month of operation and a cluster (0917, 0920, 1015, 1101) containing spectra recorded after 45 days of operation and later. This later cluster had a spectral distance of 0.45 from the starting cluster. This may indicate a change in the bacteria of Type-II between the 30th and the 45th day of operation.

In order to gauge the significance of the spectral distances seen in Fig. 9, another HCA was performed with resonant Raman spectra of individual cells from *N. communis* (Nm-02), two strains of *N. europaea* (Nm-50, Nm-53), and the carotenoids-free mutant DSM 2340^{T} of *R. sphaeroides* in pure culture (data not shown). The resulting dendrogram showed spectral distances of 0.16–0.19 between spectra belonging to the same strain, a spectral distance of 0.44 between strains of the same species (*N. europaea*), and a spectral distance of 0.58 between different species holding the same chromophore (*N. communis* and *N. europaea*). For comparison, the spectra of bacteria holding a chromophore slightly variant from heme-c – like heme-cbb$_3$ in cytochrome-cbb$_3$ expressed by the carotenoids-free mutant of *R. sphaeroides* – are at a spectral distance larger than 1 to those of bacteria expressing heme-c.

3.4. *Bacterial identification – who's who?*

The first bacterial fingerprint (Type-I) recorded from the seed mass was identified with 94% certainty as *N, communis* Nm-02 grown in planctonic culture by OPUS IDENT as described

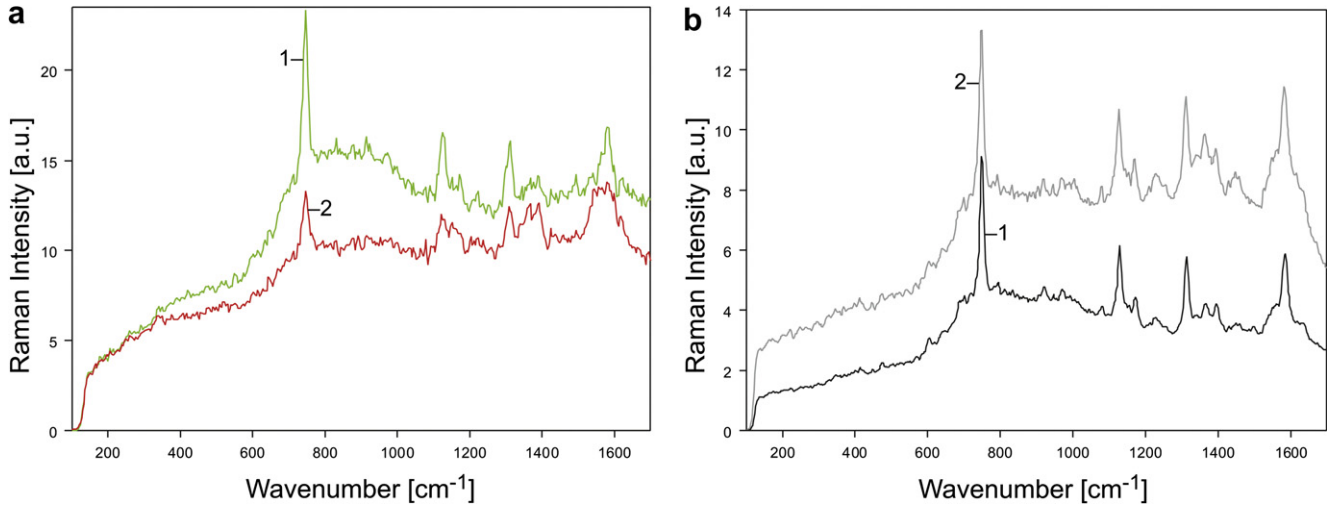

Fig. 8 – Resonant Raman spectra of bacteria containing cytochrome-c as main chromophore: type-I (a1) and type-II (a2) as recorded in the seed granules obtained from Rotterdam and *Nitrosomonas communis* Nm-02 (b1) and *Nitrosomonas europaea* Nm-50 (b2) as recorded from pure planctonic cultures.

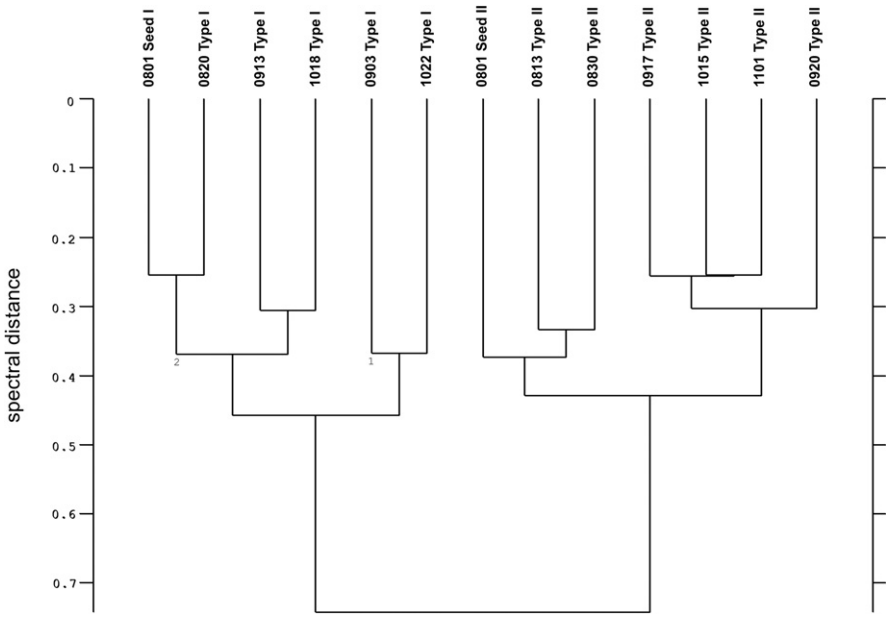

Fig. 9 – Hierarchical cluster analysis as described in 2.4 of resonant Raman spectra extracted from spectral images of the outer layer of anammox granules. Spectra are marked by date of measurement (month-day) and type as identified by the fingerprint filter. Seed I and II were found in the outer layer of the anammox seed mass.

in 2.5. Spectrum comparison between the second bacterial fingerprint (Type-II) and the other available reference spectra found a best match with a spectral similarity of approx. 80% to several *N. europaea* references (Nm-50, Nm-53), indicating a different strain of *N. europaea* or a phenotype variant from the phenotype observed in planctonic culture. Bacteria of this type were typically found surrounded by *N. communis* as identified by reference from planctonic culture (Type-I) and seldom or never had contact to water-rich areas of the active layer.

For comparison, resonant Raman spectra recorded from individual cells of a pure culture as analyzed for the reference dendrogram in 3.3 are identified with 96 ± 4% certainty when compared to spectra of the same strain and with 84 ± 5% certainty when compared to spectra of a different strain of the same species. The spectral similarity to bacteria expressing heme-cbb$_3$ instead of heme-c was typically 60% or less. The uncertainties decrease significantly with stricter limitation of the spectrum quality (i.e. allowing a narrower band of S/N ratios in spectra submitted to HCA).

4. Discussion

The identity of the chromophores found in the samples were confirmed by their Raman spectra as reported by Koyama (1995) (carotenoids), Hu et al. (1993) (cytochrome-c), and Varotsis et al. (1995) (cytochrome-cbb$_3$; solely in reference cultures of purple bacteria).

4.1. *Outer layers*

The characteristics observed by confocal resonance Raman micro-spectroscopy without prior knowledge about the samples are in very good agreement with the results of several other groups investigating similar bacterial aggregates and biofilms with conventional methods (Sliekers et al., 2002; Gieseke et al., 2003; Nielsen et al., 2005; Okubo et al., 2006; Tsushima et al., 2007). In detail:

4.1.1. *SBR-1: nitrifying layer on anammox granules*

The existence of a structured nitrifying layer of approx. 20–30 μm thickness (up to 100 μm) – as seen in Figs. 4 and 7 – on the surface of anammox granules of similar size was already reported by Nielsen et al. (2005), testing indiscriminant for *Nitrosomonas* (*N. europaea*, *N. eutropha*, *Nitrosococcus mobilis*, *Nitrosomonas halophila*) and betaproteobacterial aerobic ammonium oxidizers in general. While Nielsen et al. did not discuss canals and microcolonies present, both are clearly visible in their presented data obtained with FISH of paraformaldehyde (PFA)-fixed cryosections of sampled aggregates.

In addition, confocal (resonance) Raman micro-spectroscopy revealed the nitrifying layer of granules sampled from our sequencing batch reactor with nominal anammox activity (SBR-1) as a dense multilayer of at least two different nitrifying bacteria species – *N. communis* and a second species (probably *N. europaea*) – forming microcolonies in distinct spatial relation, with the second species typically not having contact to bulk liquid or water-filled canals. Co-existing microcolonies of different nitrifying bacteria (*N. europaea/eutropha*, *N. mobilis*) associated on the microscale were previously reported for example by Gieseke et al. (2003), who employed CLSM in combination with FISH on PFA-fixed thin sections.

HCA of the obtained Raman spectra indicated that a change occurred in the second species of *Nitrosomonas* between 30 and 45 days after inoculation, coinciding with the

time after which denitrification continuously exceeded anammox in SBR-1 according to Wesoly (2009). Similar time frames for biomass adaptation to changed environmental conditions were reported for example by Tsushima et al. (2007) for the simultaneous removal of ammonium and nitrite being detectable after startup, and Sliekers et al. (2002) for the formation of biomass containing 45% aerobic ammonium oxidizers, primarily *Nitrosomonas*, after aeration of a previously strict anoxic SBR. At this point in time, we may only speculate about the observed change detected in the second *Nitrosomonas* species to be the result of phenotypic adaptation to the by then established local microenvironment (Steward and Franklin, 2008) between the dense colonies of *N. communis* separating them from the bulk water.

4.1.2. *SBR-0: purple bacteria*

Confocal resonance Raman micro-spectroscopy distinguished two different types of bacteria in the outer layer of SBR-0. Bacteria producing carotenoids with a neurosporene backbone were found typically in contact with bulk water or on the walls of water-filled gaps, while bacteria within the microcolonies produced carotenoids with a spheroidene backbone. Carotenoids are ubiquitous chromophores, which in phototrophic bacteria are mostly associated with the light harvesting complexes (Cogdell et al., 2006). Since both carotenoids are intermediates of the spheroidene pathway for the biosynthesis of carotenoids typical in phototrophic purple bacteria (Takaichi, 2008), we cannot decide at this point in time whether or not the variant chromophores are indicative of two different species of purple bacteria (Okubo et al., 2006), or are in fact indicative of an adaptation of the same species to different habitat conditions in the biofilm (Steward and Franklin, 2008), e.g. stopping the carotenoid synthesis at neurosporene when in contact to bulk water, instead of continuing down the synthesis pathway towards spheroidene.

However, Pudney et al. (2011) successfully traced the molecular status of multiple carotenoids in tomatoes and tomato products with confocal Raman micro-spectroscopy. Given the complexity of the carotenoid composition found in many bacteria (Takaichi, 2008a), a species-sensitive detection based on present carotenoids, carotenoid associations and conformations may well be possible.

4.1.3. *TiO_2 microparticles and bacteria*

The exact origin of the TiO_2 microparticles found in the samples is unknown as they were not specifically added to the SBRs. However, it is highly likely that municipal wastewater used in the startup process and in the cyclic feeding of the SBRs contained noticeable traces of them, given that TiO_2 in rutile phase is widely used as a white pigment even in foods (E171) and anatase is used for example as optical brightener in plastics (Fink, 2010).

The location of the TiO_2 microparticles with respect to the purple bacteria in the outer layer of granules sampled from SBR-0 appears to be mineral phase dependent. Microparticles of TiO_2 in anatase phase were not in direct contact to bacterial microcolonies and often stuck in thick swaths of low density matter, which might be comparable to the gelatinous matrix seen in mats of phototrophic non-sulfur purple bacteria reported by Okubo et al. (2006). Rutile microparticles were typically densely populated with purple bacteria appearing almost embedded in large microcolonies. We are not aware of a study reporting anything comparative to this for small microparticles in the range of 1–10 μm (or anything larger). Nothing of this kind was observed in the nitrification layer of granules sampled from SBR-1.

However, Fang et al. (2010) reported anatase nanoparticles to cause cell shrinkage and membrane damage in *N. europaea*, independent of particle size (25 nm, 200 nm), while Liu et al. (2010) showed membrane damage caused in *Escherichia coli* by TiO_2, confirming bactericidal properties even in absence of UV irradiation. In addition, Johnston et al. (2009) reviewed the toxicity of TiO_2 in anatase and rutile phase on tissues and eukaryotic cells, finding the toxic potency of anatase considerably larger than that of rutile in most of the studies, some of which covered prokaryotic cells as well. This may explain while anatase microparticles embedded in the outer layer were surrounded by low density matter keeping them separated from the purple bacteria microcolonies, while rutile crystals were found overgrown. Considering the slow growth of *Nitrosomonas* in comparison to most purple bacteria and the aforementioned results of Fang et al., the toxic effects of rutile – and esp. anatase – microparticles may have a more severe impact on microcolonies of *Nitrosomonas*. This may explain why there were few rutile and virtually no anatase microparticles embedded in the nitrifying layer of granules sampled from SBR-1.

4.2. *Quantification and digital image analysis*

Sandt et al. (2008) proposed a quantitative analysis of the water-to-biomass ratio of biofilms based on the CH-stretching modes seen in EPS and biomass and the OH-stretching modes of water (centered around 2840 cm^{-1} and 3400 cm^{-1} respectively). However, in our case the water-to-biomass ratio of a single spectrum already depended highly on whether or not a bacterial cell was within the measurement volume. In addition, a statistical approach by averaging multiple spectra would have been highly arbitrary, given that discriminating between extra-cellular water in the EPS and intra-cellular water of the bacteria is not possible.

While we did not use digital image analysis for quantification on our data, the nature of the data allows straightforward employment of the technique. The bias caused by manually set thresholds (or thresholding algorithms) as described by Daims and Wagner (2007) and Merod et al. (2007) does not exist due to the inherent threshold definition of the major known Raman lines in a fingerprint spectrum to exceed the background of autofluorescence and random noise by at least a given intensity, e. g. for the S/N to satisfy an adapted Rose criterion (Bright et al., 1998).

4.3. *Resonance Raman micro-spectroscopy in comparison to other methods*

Very few techniques for blind, label-free imaging of native, undisturbed biofilm have been reported to date: most notably, infrared absorption and normal Raman spectroscopy, often in combination with confocal microscopy, have been employed for several biofilm and bacteria studies. However, long exposure times (100 s and more) and high variability of bacterial

Raman spectra due to variant environmental conditions and metabolic variants of the cells pose significant challenges for mapping biofilms as well as identifying bacteria (Sandt et al., 2007; Harz et al., 2008). In contrast, resonance Raman spectroscopy relies primarily on specific ubiquitous molecules (chromophores) produced by the bacteria. The resonant excitation of these chromophores allows for significantly shorter exposure times (1 s and less) and reduces the variability of the spectra to metabolic changes of the bacterial cell directly affecting the chromophores. However, the reliance on chromophores restricts specificity to the specificity of the chromophore within the bacteria and also dictates the excitation wavelength, thus affecting the compatibility with methods such as FISH, which require fluorescent staining (Neu et al., 2010). Most, if not all, available fluorescent stains do not allow for subsequent (resonant) Raman measurements with visible excitation. The combination of Raman and FISH reported by Huang et al. (2007) relied on the detection of ^{13}C labeled cells, trading most – if not all – of the advantages of Raman micro-spectroscopy in regard of non-invasive measurements of native, undisturbed samples.

Ivleva et al. (2010) used rapid surface enhanced Raman scattering (SERS) in combination with normal Raman for the in situ chemical characterization of complex biofilms grown on marked glass slides, mapping several SERS fingerprints indicative of polysaccharides and proteins. The presented raster maps of 60 × 60 μm^2 with a spatial resolution of 3 μm were recorded with an excitation time of 1 s per SERS spectrum, bringing this technique in the same range of spatial resolution and recording time as resonance Raman measurements. However, the requirement of silver nanoparticles as SERS substrate may limit this technique to endpoint analyses, given that silver nanoparticles of similar size have been reported by Liang et al. (2010) to have a severe negative impact on nitrifying bacteria in activated sludge, leading to significant nitrification inhibition and changes in the communal composition of the present bacteria.

Haisch and Niessner (2007) reported on optical coherence tomography (OCT) for online, in vivo and in situ visualization of three-dimensional biofilm density structures with a 10 μm resolution and transient processes with an impressive temporal resolution between 1 s and a few minutes for complete images. However, while discrimination between bacterial matter and larger microparticles (diameter >10 μm) and even different types of microparticles may be possible due to different particle densities, the discrimination between different types of bacteria and thus the subsequent identification of bacteria as shown with resonance Raman micro-spectroscopy is not possible with OCT. A combination of OCT and CLSM as reported by Wagner et al. (2010) for analyzing comparatively large swaths of biofilm (sample volumes of 4 × 4 × 3 mm^3 at a resolution below 20 μm), gives hope for the successful combination of OCT with (resonance) Raman micro-spectroscopy in the future.

5. Conclusion

We successfully demonstrated the suitability of confocal (resonance) Raman micro-spectroscopy for blind in vivo analysis of the first 80 μm of undisturbed biofilms in water. The analysis covered structural information and distribution, tracking, and identification on the scale of single bacterial cells. Microparticles embedded in the outer layer were also successfully analyzed with respect to the mineral phase and the surrounding bacterial microcolonies.

Confocal (resonance) Raman micro-spectroscopy has the following key features:

- non-invasive optical analysis of living, undisturbed wet samples (no fixation, probes, labels, or stains required) of up to 80 μm thickness
- blind measurements (no advance knowledge required; chromophores can be identified after the measurement; background analysis prevents false negatives)
- spatial resolution at cell size (0.35 μm^2 × 2 μm) or (0.35 μm^2 × 1.2 μm), allowing quantification at absolute cell numbers if required, with excitation times of 0.5–1.0 s for a single spectrum (0.1 s for single wavelength detection in 3D)
- identification of bacteria in genus, strain and/or phenotype (dependent on chromophore), distribution and tracking of bacteria independent from identification
- biological and mineral components can be analyzed in the same measurement

Acknowledgments

This work was kindly supported by the German Research Foundation (DFG, grant no. AN 712/1-5).

The authors would like to thank Dr. Andreas Pommerening-Röser of the Biozentrum Klein Flottbek, Mikrobiologie und Biotechnologie, in Hamburg for providing us with the *Nitrosomonas* references and invaluable information about their cultivation.

The authors would like to express special thanks to Dr. Ilona Wesoly for detailed information on the starting conditions and operation of the SBRs.

The help of Dipl.-Biol. Tobias William Gaul in cultivating the *Nitrosomonas* references is kindly acknowledged.

REFERENCES

Bright, D.S., Newbury, D.E., Steel, E.B., 1998. Visibility of objects in computer simulations of noisy micrographs. Journal of Microscopy 189 (1), 25–42.

Cogdell, R.J., Gall, A., Köhler, J., 2006. The architecture and function of the light-harvesting apparatus of purple bacteria: from single molecules to *in vivo* membranes. Quarterly Reviews of Biophysics 39 (3), 227–324.

Daims, H., Wagner, M., 2007. Quantification of uncultured microorganisms by fluorescence microscopy and digital image analysis. Applied Microbiology Biotechnology 75, 237–248.

Downs, R.T., 2006. The RRUFF Project: an Integrated Study of the Chemistry, Crystallography, Raman and Infrared Spectroscopy of Minerals Program and Abstracts of the 19th General Meeting of the International Mineralogical Association in Kobe, Japan03–13.

Fang, X., Yu, R., Li, B., Somasundaran, P., Chandran, K., 2010. Stresses exerted by ZnO, CeO_2, and anatase TiO_2 nanoparticles on the *Nitrosomonas europaea*. Journal of Colloid and Interface Science 348, 329–334.

Fink, J.K., 2010. A Concise Introduction to Additives for Thermoplastic Polymers. Scrivener Publishing, LLC, Salem, Massachusetts.

Gieseke, A., Bjerrum, L., Wagner, M., Amann, R., 2003. Structure and activity of multiple nitrifying bacterial populations co-existing in a biofilm. Environmental Microbiology 5 (5), 355–369.

Haisch, C., Niessner, R., 2007. Visualisation of transient processes in biofilms by optical coherence tomography. Water Research 41, 2467–2472.

Harz, M., Rösch, P., Popp, J., 2008. Vibrational spectroscopy – a powerful tool for the rapid identification of microbial cells at the single-cell Level. Cytometry Part A 75A, 104–113.

Hu, S., Morris, I.K., Singh, J.P., Smith, K.M., Spiro, T.G., 1993. Complete assignment of cytochrome c resonance Raman spectra via enzymic reconstitution with isotopically labeled hemes. Journal of the American Chemical Society 115 (26), 12446–12458.

Huang, W.E., Stoecker, K., Griffiths, R., Newbold, L., Daims, H., Whiteley, A.S., Wagner, M., 2007. Raman-FISH: combining stable-isotope Raman spectroscopy and fluorescence in situ hybridization for the single cell analysis of identity and function. Environmental Microbiology 9 (8), 1878–1889.

Ivleva, N.P., Wagner, M., Szkola, A., Horn, H., Niessner, R., Haisch, C., 2010. Label-free in situ SERS imaging of biofilms. Journal of Physical Chemistry B 114, 10184–10194.

Johnston, H.J., Hutchison, G.R., Christensen, F.M., Peters, S., Hankin, S., Stone, V., 2009. Identification of the mechanisms that drive the toxicity of TiO_2 particulates: the contribution of physicochemical characteristics. Particle and Fibre Toxicology 6 (33). doi:10.1186/1743-8977-6-33.

Kniggendorf, A.-K., Gaul, T.W., Meinhardt-Wollweber, M., 2011. Effects of ethanol, formaldehyde, and gentle heat fixation in confocal resonance Raman microscopy of purple nonsulfur bacteria. Microscopy Research and Technique 74, 177–183.

Kniggendorf, A.-K., Gaul, T.W., Meinhardt-Wollweber, M., 2011a. Hierarchical cluster analysis (HCA) of microorganisms: an assessment of algorithms for resonance Raman spectra. Applied Spectroscopy 65 (2), 165–173.

Koops, H.-P., Böttcher, B., Möller, U.C., Pommerening-Röser, A., Stehr, G., 1991. Classification of eight new species of ammonia-oxidizing bacteria: Nitrosomonas communis sp. nov., Nitrosomonas ureae sp. nov., Nitrosomonas aestuarii sp. nov., Nitrosomonas marina sp. nov., Nitrosomonas nitrosa sp. nov., Nitrosomonas eutropha sp. nov., Nitrosomonas oligotropha sp. nov. and Nitrosomonas halophila sp. nov. Journal of General Microbiology 137, 1689–1699.

Koyama, Y., 1995. In: Britton, G., Liaaen-Jensen, S., Pfander, H. (Eds.), Carotenoids Volume 1B: Spectroscopy, (chapter 5): Resonance Raman Spectroscopy. Birkhäuser Verlag, Basel, pp. 135–146.

Liang, Z., Das, A., Hu, Z., 2010. Bacterial response to a shock load of nanosilver in an activated sludge treatment system. Water Research 44, 5432–5438.

Liu, P., Duan, W., Wang, Q., Li, X., 2010. The damage of outer membrane of *Escherichia coli* in the presence of TiO_2 combined with UV light. Colloids and Surfaces B: Biointerfaces 78, 171–176.

Merod, R.T., Warren, J.E., McCaslin, H., Wuertz, S., 2007. Toward automated analysis of biofilm architecture: bias caused by extraneous confocal laser scanning microscopy images. Applied and Environmental Microbiology 73 (15), 4922–4930.

Neu, T.R., Manz, B., Volke, F., Dynes, J.J., Hitchcock, A.P., Lawrence, J.R., 2010. Advanced imaging techniques for assessment of structure composition and function in biofilm systems. FEMS Microbiology Ecology 72, 1–21.

Nielsen, M., Bollmann, A., Sliekers, O., Jetten, M., Schmid, M., Strous, M., Schmidt, I., Hauer Larsen, L., Nielsen, L.P., Revsbech, N.P., 2005. Kinetics, diffusional limitation and microscale distribution of chemistry and organisms in a CANON reactor. FEMS Microbiology Ecology 51, 247–256.

Okubo, Y., Futamata, H., Hiraishi, A., 2006. Characterization of phototrophic purple nonsulfur bacteria forming colored microbial mats in a swine wastewater ditch. Applied and Environmental Microbiology 72 (9), 6225–6233.

Pudney, P.D.A., Gambelli, L., Gidley, M.J., 2011. Confocal Raman microspectroscopic study of the molecular status of carotenoids in tomato fruits and foods. Applied Spectroscopy 65 (2), 127–134.

Sandt, C., Smith-Palmer, T., Pink, J., Brennan, L., Pink, D., 2007. Confocal Raman microspectroscopy as a tool for studying the chemical heterogeneities of biofilms in situ. Journal of Applied Microbiology 103, 1808–1820.

Sandt, C., Smith Palmer, T., Pink, J., Pink, D., 2008. Quantification of local water and biomass in wild type PA01 biofilms by confocal Raman microspectroscopy. Journal of Microbiological Methods 75, 148–152.

Schwartz, T., Jungfer, C., Heißler, S., Friedrich, F., Faubel, W., Obst, U., 2009. Combined use of molecular biology taxonomy, Raman spectrometry, and ESEM imaging to study natural biofilm grown on filter materials at waterworks. Chemosphere 77, 249–257.

Sliekers, A.O., Derwort, N., Campos Gomez, J.L., Strous, M., Kuenen, J.G., Jetten, M.S.M., 2002. Completely autotrophic nitrogen removal over nitrite in one single reactor. Water Research 36, 2475–2482.

Steward, P.S., Franklin, M.J., 2008. Physiological heterogeneity in biofilms. Nature Reviews Microbiology 6, 199–210.

Takaichi, S., 2008. In: Hunter, C.N., Daldal, F., Thurnauer, M.C., Beatty, J.T. (Eds.), Advances in Photosynthesis and Respiration Vol. 28: The Purple Phototrophic Bacteria, (Chapter 6)-II: Carotenogenesis. Springer, Dordrecht, The Netherlands, pp. 101–111.

Takaichi, S., 2008a. In: Hunter, C.N., Daldal, F., Thurnauer, M.C., Beatty, J.T. (Eds.), Advances in Photosynthesis and Respiration vol. 28: The Purple Phototrophic Bacteria, (Chapter 6)-III: Carotenoids in Purple Bacteria. Springer, Dordrecht, The Netherlands, pp. 111–117.

Tsushima, I., Ogasawara, Y., Kindaichi, T., Satoh, H., Okabe, S., 2007. Development of high-rate anaerobic ammonium-oxidizing (anammox) biofilm reactors. Water Research 41, 1623–1634.

Van der Star, W.R.L., Miclea, A.I., van Dongen, U.G.J.M., Muyzer, G. , Picioreanu, C., van Loosdrecht, M.C.M., 2008. The membrane bioreactor: a novel tool to grow anammox bacteria as free cells. Biotechnology Bioengineering 101, 286–294.

Varotsis, C., Babcock, G.T., Garcia-Horsman, J.A., Gennis, R.B., 1995. Resonance Raman spectroscopy of the heme groups of cytochrome cbb3 in rhodobacter sphaeroides. Journal of Physical Chemistry 99 (46), 16817–16820.

Wagner, M., Ivleva, N.P., Haisch, C., Niessner, R., Horn, H., 2009. Combined use of confocal laser scanning microscopy (CLSM) and Raman microscopy (RM): investigation on EPS-Matrix. Water Research 43, 63–76.

Wagner, M., Taherzadeh, D., Haisch, C., Horn, H., 2010. Investigation of the mesoscale structure and volumetric features of biofilms using optical coherence tomography. Biotechnology and Bioengineering 107 (5), 844–853.

Wesoly, I. 2009. Operating Strategies for the anammox process in sequencing batch reactors (German). Doctoral thesis. Technical University of Berlin, Germany.